POLITECNICO DI MILANO
School of Industrial and Information Engineering
Master of Science in Telecommunication Engineering

POLITECNICO
MILANO 1863

Study of an Optomagnetic Biosensor in Integrated Photonics

Supervisor : Prof. Andrea Melloni
Co-supervisor : Dr. Piero Borga

Master thesis of :
Jalal Babaeian
ID: 926790

Academic year 2020/2021

Contents

List of Figures

Abstract

Bio sensing will help us in detection of smallest biological events such as DNA hybridization, antibody-antigen interaction or protein-protein interactions and several other biological events that are important for diagnostics. The presence and availability of a biosensor will help patients to monitor their own health condition in order to take care of their own lives. Availability of a biosensor so that everyone can use it is not possible without integration of the whole system. The system must be effective, efficient, packed, integrated, and easy to work with. In this study we suggest a new configuration for biosensing using photonic micro ring resonator that uses active labelling for detection. Optomagnetic sensing which is the result of active labelling using ferromagnetic labels will lead us to have coherent detection that greatly improves the sensitivity. This study discusses about the possible ways of integration of the optomagnetic biosensors. Our mainly focus is on finding the optimum configuration of the magnetic coils integrated with MRR inside a single chip that provides our desired magnetic force and angle to reach the highest efficiency for the biosensors.

Introduction

In the field of biosensing we use micro ring resonator in order to sense and track smallest biological events such as DNA hybridization and the interactions of protein with protein or antibody with antigen or vice versa. Passively labelling the analytes will increase the outcome of the sensor; however, it is not enough for very low concentration of analytes. This is why we use active labelling approach where we use a magnetic bead as an active label in order to provide the possibility of increasing the resonance wavelength shift by applying a magnetic force on the bead. Active labelling will provide the possibility of retrieving an external signal due to the fluctuations of the label in presence of a magnetic field. In this study we consider a new structure for optomagnetic sensing which is based on the interaction between the ferromagnetic bead bound to the sensing analyte and the magnetic coils integrated inside a single chip with the micro ring resonators. This integration will increase the effectiveness and the efficiency of the biosensor. Five different structures have been proposed in this thesis for the configuration of the magnetic coils inside the photonic chip which are almost all the possible ways for integration. Since we have studied all the configurations possible, we can confidently say that the final structure for the magnetic coils has not been chosen randomly. The optimization path for choosing the best integrated magnetic coil structure has been chosen by considering the maximum force each structure can provide, the angle of the force on the surface of the MRR that is applied on the ferromagnetic bead, and the implementation process. The angle and the force value of the final structure are enough to completely bend DNA so that the bead gets to the closest point to the surface of the MRR.

Chapter 1- We will describe what bio sensing with photonic micro ring resonator (MRR) means, and why active labelling will result in better performance.

Chapter 2- We investigate the impact of magnetic nano particles (MNP) on the electromagnetic field and test the micro ring behaviour in presence of MNP. Later in this chapter we will study the mechanical properties of DNAs in order to see how they bend over a curvature if we apply force to the bead. This is important as we want to know what amount of magnetic force we must produce.

Chapter 3- In this chapter we will design a structure that can provide the magnetic force required to push down the bead. We need to consider the amount of force needed which we have obtained in chapter 2, and the idea of integration inside a single chip where the MRR is present.

Chapter 4- In this chapter we will focus on how we can implement the testing. We designed a photonic board to hold the photonic chip and the fluidic cell.And an

electronic board used to acquire data from the photodiodes and apply current to the magnetic coils.

Chapter 1

Biosensing in Integrated Photonics

1.1 Photonic Biosensor and State of Art

This thesis is about a particular type of biosensors that uses micro ring resonator in silicon photonics technology as a tool to detect and track biological events. Optical biosensors are realized in different technologies such as Surface Plasmon Resonance (SPR) [1] and Photonic Crystals [2]. Today due to the improvement of our knowledge in silicon photonics and the availability of multi wafer projects, researchers have promising opportunities to access high quality resonating cavities as a device for detection at low cost. The only full integrable circuit among different resonating cavities is micro ring resonator.

Thanks to Covid 19, we are generally very much familiar with viruses and their diagnosis. HIV for example can be possibly cured if it is detected at the very first days of its presence in our body. The concentration of virus in our body at the starting point is very low that can not be easily identified. We have begun a journey in detecting very small biological events that they were not used to be detected or sensed by any doctor or any sensor. For convenience we have chosen DNA bindings as our event to be studied and sensed.

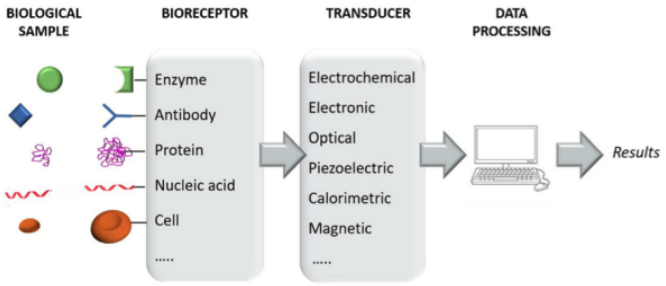

Figure 1.1: Building blocks of biosensors. We use nucleic acid receptor and optical transducer

Any biosensor has a biochemical receptor and a transducer that yields a signal which must be proportional to the concentration of a particular chemical. The event we want to study is binding of the DNA. The receptor is a single stranded DNA (ssDNA), the set of chemicals are the matching single stranded DNAs with the receptors and the transducer can be said to be the photonic micro ring resonator that converts the concentration of the matching ssDNAs into a photonic signal which is

further transformed into electronic signals using photodiodes. the builing blocks of our system are 1- DNA bindings 2- Photonic micro ring resonator (photonic MRR)

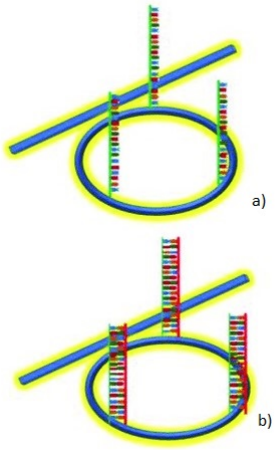

Figure 1.2: a) receptors with single stranded DNA b) matching ssDNA bound to receptor

1.2 Micro Ring Resonator for Biosensing

photonic MRR is a photonic device that can have either 2 or 4 ports [3]. The input light confined in a waveguide has an evanescent field so it is better to say light does not only see the material inside the core of the waveguide; however, it also sees the environment around the core. Effective refractive index which is a kind of material characteristics is what light is moving with respect to inside a waveguide. it is a value between the refractive index of the core and the cladding. the more the light is confined inside the core the closer the effective refractive index (n_{eff}) is to the refractive index of the core. Due to the evanescent field light can be coupled to another waveguide or a ring which is dependent on the coupling coefficient between the two structures.

The light that we emit has a range of frequency. if we couple the waveguide with a ring according to eq.1.1 dependant on the radius of the ring and the effective refractive index a frequency remains inside the cavity (ring).

$$m\lambda = 2\pi r n_{eff} \tag{1.1}$$

$2\pi r$ is the perimeter of the ring and m is any arbitrary integer number.

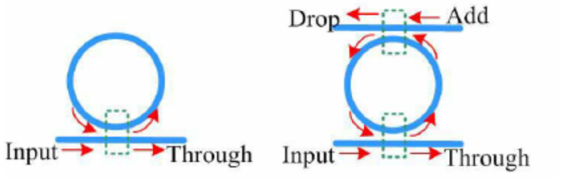

Figure 1.3: two port micro ring resonator and four port micro ring resonator

The resonance frequency is dependent on the effective refractive index and we already know that n_{eff} is dependant on $n_{cladding}$ and n_{core}. If we remove the cladding

of the waveguide then we can say the surrounding of the core will be visible by the evanescent field, therefore n_{eff} will be dependant on the surrounding materials of the core which means the bound DNAs are visible by the light and are playing a role in foundation of the effective refractive index which indicates the resonance frequency by eq.1.1.

The 2 port MRR can not be designed in order to have high ER or it is very difficult to do so. This is why we are willing to use a 4 port MRR where the power remained inside the cavity can exit at the drop port. see fig 1.4.

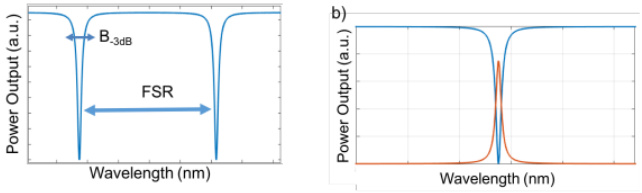

Figure 1.4: four and two port micro ring resonator frequency spectrum

We want to detect the binding process of DNA and we concluded that the resonance wavelength has this information. Consider an MRR that receptor ssDNAs are bound on the surface of the ring on top of the core. the surrounding of the core is a solution which its refractive index is stable. In this case the wavelength frequency has a specific value. Now slowly change the refractive index of the solution by injecting the matching ssDNAs. If we stay a fair period of time after the last ssDNA we injected into the solution (to reach the steady state) we can see the resonance wavelength has been shifted slightly. The resonance shift indicates the concentration of the binding DNAs at the steady state. If we observe and write down the wavelength resonance meanwhile the process is going on then we can not only see the final resonance shift, but also we can see and track the DNA binding process which is interesting.

This assumptions are very perfect since we are not sure whether the refractive index of the solution without the DNAs remain stable during our observation process. The noises as thermal fluctuation are not also considered in this assumption. Therefore we need to duplicate our system and name them as sensing MRR and reference MRR. On the reference MRR we only detect and track the refractive index changes of the solution without any chemicals. see fig 1.5.

In this scenario the wavelength shift is very small. After the process of binding we can add another step. By injecting heavy material with high refractive indexes that can bind to the complete DNAs we can change the effective refractive index a lot. We call this material as "bead". By this approach apart from increasing n_{eff} we are actually labelling the completely bound DNAs, which means we are precisely sensing what we want. This scenario is called label-based approach. By Using label based approach the resonance wavelength shifts significantly and can be detected even with less concentration of completely bound DNAs. see fig 1.6.

1.3 Optomagnetic Technique

Biosensors can be generally classified in label free and labelled approaches. In label free the analyte is the only factor for detection. Labelling the analyte can be done

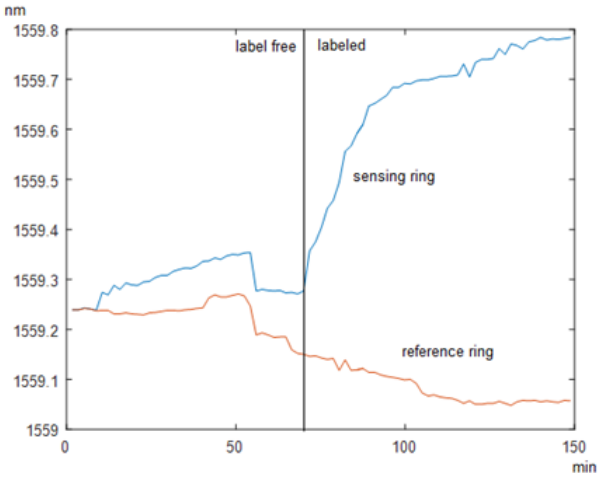

Figure 1.5: Real observation on the reference ring and the sensing ring

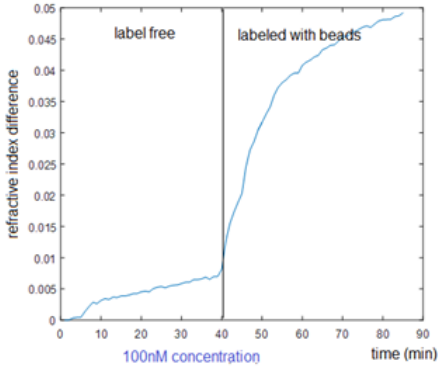

Figure 1.6: Δn_{eff} in label free and label based approaches in 100nM concentration

either passively and actively. Passive labelling will increase the refractive changes of the solution more that label free approach since normally the label which is used has bigger dimension in comparison with the analyte alone. When we use a specific label with particular characteristics which will lead us to produce an external observable signal is called active labelling. In our case the label is a magnetic bead that can oscillate in presence of a magnetic field.

We saw in fig 1.6 that with concentration of 100nM we can detect the wavelength shift clearly and we can track the binding process well enough. However if we go below 0.1nM then we can not clearly extract the wavelength shift. If we use a bead with ferromagnetic properties, we can force down the bead close to the core of the ring resonator in order to apply more refractive index variation. Since the bead is chosen to be ferromagnetic therefore the force that can push it down can be generated by a magnetic field. The main improvement in using a magnetic bead is the use of coherent detection which will increase the robustness of the biosensor.

Consider after a lot of measurements we come up to a calibration curve that by looking at it we can say for set of different concentrations we have a set of different wavelength shifts. The coil we have installed outside will prevent us from having a reliable look up table. This happens because we can not be sure if we have placed the magnetic coil for our new experiment exactly similar to where we had placed before. If this happens then the wavelength shift would be dependant on the location

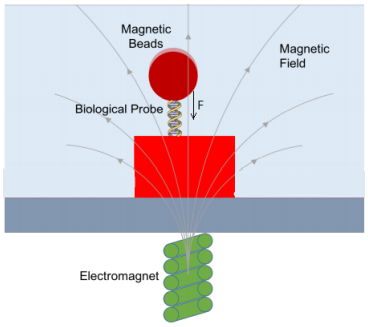

Figure 1.7: magnetic force applied to the magnetic bead by a magnetic coil

that we have placed the magnetic coil. So an important figure of merit for sensors is integration and we want to have the magnetic coil and the ring resonators that are for sensing to be integrated into a single chip.

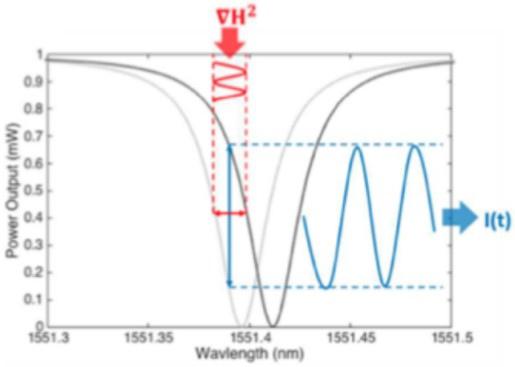

Figure 1.8: Active labelling

What we are willing to do is bending down the DNA with a magnetic field in order to have the bead at the closest point to the surface of the MRR. Assume we are reading a single frequency on the notch (see fig 1.8) where its slope is maximum. By shifting the resonance wavelength due to DNA bending which will result in refractive index changes we will increase the intensity. With coherent detection we will increase the robustness of the biosensor and in this study we will introduce an integrated optomagnetic biosensor which will increase the reliability, robustness, compactness, and precision.

The optomagnetic detection technique reduces the measurement time to few seconds in comparison with the other configurations. Because optomagnetic technique offers the opportunity to obtain a signal only when the magnetic field is applied. As it is depicted on the left side of fig.1.9 this technique will cause error in low concentration of analytes around 100[pm]. The integrated system we introduce in chapter 4 will increase the robustness to the error.

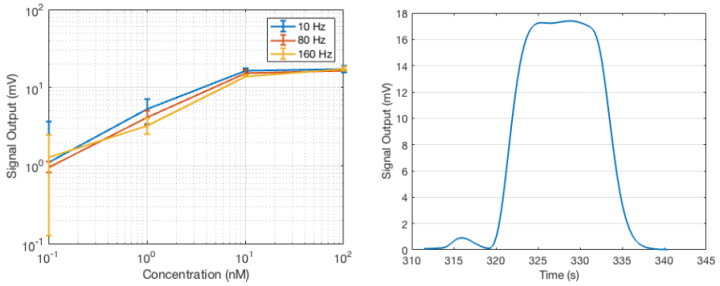

Figure 1.9: On the left typical on-off signal acquired with the opto-magnetic platform is depicted (100 nM concentration of DNA). On the right the output signal with respect to different on-off frequency and concentrations have been illustrated

1.4 Summary of Results

Optomagnetic technique which is an active labelling type of biosensing will help us in producing an external signal coming from the fluctuation of the bead which is robust to the incoming noise from detection of the wavelength shift. Integrating the optomagnetic technique which is the integration of the magnetic coils and the micro ring resonators inside a single chip will bring the idea of widely usage of optomagnetic biosensors down on earth. The fact that integration will enhance the precision of the sensing is another reason that this thesis is mainly focused on optomagnetic biosensing in integrated photonics. Every measurement will be dependant on the accuracy of the placement of the magnetic coils if the magnetic coils are not integrated inside the photonic chip. Which means we can not rely with confidence on the outcome signals and information they reveal. We have taken a very big step forward to the integration of optomagnetic biosensors by designing a chip that contains both the MRR and the magnetic coils which increases the precision, reliability and robustness to the noise.

Five different structures have been proposed in this thesis for the configuration of the magnetic coils inside the photonic chip which are almost all the possible ways for integration. Since we have studied all the configurations possible, we can confidently say that the final structure for the magnetic coils has not been chosen randomly. The optimization path for choosing the best integrated magnetic coil structure has been chosen by considering the maximum force each structure can provide, the angle of the force on the surface of the MRR that is applied on the ferromagnetic bead, and the implementation process. The angle and the force value of the final structure are enough to completely bend DNA so that the bead gets to the closest point to the surface of the MRR. This will increase the amplitude of the oscillation of the light intensity at the photodiodes which will enhance our detection precision for even very low concentration of analytes in the sensing solution.

Chapter 2

Resonator and Molecule Modelling

2.1 Optical Microring Resonator

We are willing to track the resonance wavelength as an indicator of the outgoing process that we want to detect or sense. This means the notch in fig 1.4 must be very sharp. In order to have a sharp notch with high ER we need to have a very small coupling length. We have chosen a ring with 40um radius in order to have low coupling coefficient. The micro ring resonator is designed in order to be optimum for TM mode injection. We used "Comsol Multiphysics" as a tool for simulating our microring resonator in order to extract its characteristics. 3D simulation of a complete ring resonator was not efficient since it occupies a lot of memory and consumes a lot of time of operation. Since we are working with a resonating structure, the simulator will crash since it does not understand when to stop the resonating loop. When we have a loop that never ends or ends after a lot of time, the RAM in the computer as the most important resource, should be large enough to record and save the meanwhile results of the solver. Therefore simulating the whole micro ring resonator in 3D will require a lot of resources. Therefore we decided to keep going on simulating a full microring resonator in 2D where z axis is missing.

The model is a ring resonator with ring radius of 40um and coupling gap of 250nm with core width equal to 500nm and cladding width of 5um. The materials that are used for core and cladding are silicon and silicon oxide with refractive indexes of n_{core}= 3.40 and n_{clad}= 1.52.

For the couplers between waveguide and the MRR the phase of the light that is propagating in the straight waveguide is $\phi = \beta y$ if we consider the vertical axis in fig 2.1 as y axis. However, the phase that light is propagating within the ring is $\phi = \beta R arctan(-y/x)$, if we consider the horizontal axis in fig 2.1 to be x and R to be the ring radius. We know that at the coupling length the phase of the straight waveguide and the ring must be equal for the field continuity.

$$\phi = \beta y = \beta R \arctan(-y/x) \tag{2.1}$$

so we have to define the variable ϕ for the field continuity at the gap to let light couple inside the ring. And this must be applied to the other coupler too.

The MRR is in Add-Drop configuration therefore it has 4 ports. In fig 2.1 only the excitation port has been demonstrated. The type of excited field is numeric with power p0 and with phase equal to zero at the starting point.

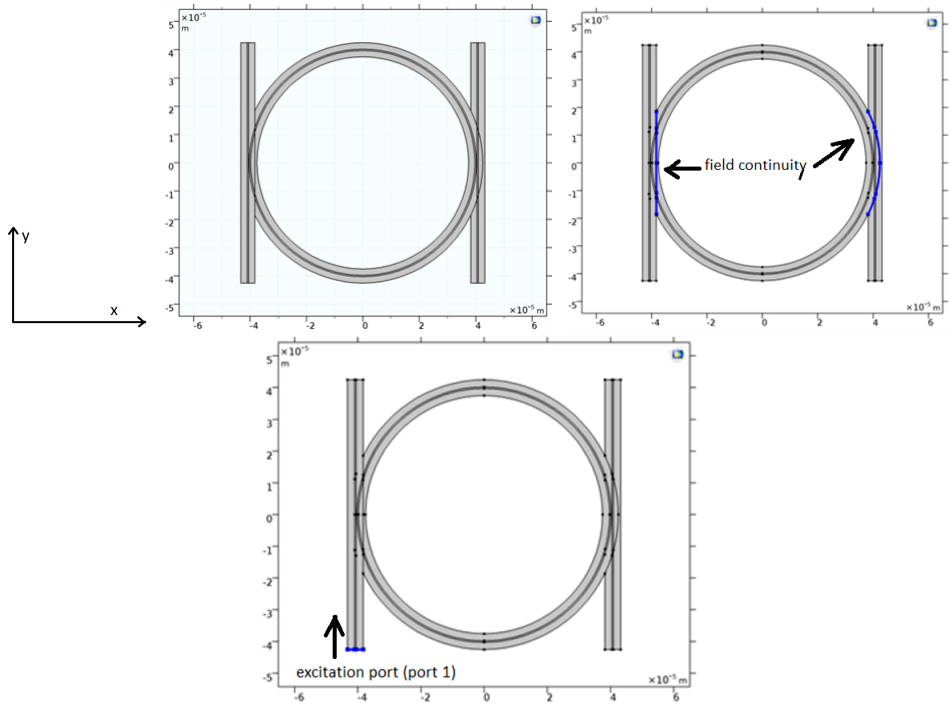

Figure 2.1: MRR dimensions and geometry: ring radius=40um, coupling gap=250nm, core width= 500nm and cladding width=5um

After simulating in electromagnetic wave and beam envelope "EWBE", what we obtain is the following spectrum in fig.2.2 By sweeping the refractive index of the cladding which is supposed to be the surrounding environment of the core we can obtain the sensitivity. Sensitivity is a very important figure of merit in biosensors that in our case is the amount of wavelength shift due to the amount of effective refractive index changes. The notch is not symmetric since there are two couplers that are not perfectly the same characteristics.

$$S = (\Delta\lambda)/(\Delta n_{cladding}) \tag{2.2}$$

Sweeping the cladding refractive index from 1.50 to 1.52 will result in Sensitivity of $20nm/RIU$. The sensitivity we expected was higher; however, we put in mind that the obtained S in this 2D simulation can be reasonable since we are not considering the z axis

On one hand simulating in 2D is not sensitive to the refractive index changes in z direction therefore we need a 3D simulating in order to retrieve the correct sensitivity. On the other hand simulating complete ring resonator is very memory and time consuming as we discussed before. Therefore I simulated a straight waveguide with similar dimensions to obtain the correct effective refractive index. Then it is possible to calculate the resonating lambda using eq.1.1.

The model is a straight waveguide with core width of 500nm, cladding width of 2.5um and cladding heigth of 1.1um. The materials used for the core is silicon, for cladding we use water solution and for substrate we use SiO2.

Electromagnetic waves and beam envelope is used for the physics of our simulation model. Since we are simulating the beam envelope, meshing in y direction doesn't need to have a lot of elements. In this model we have E0 and H0 as input

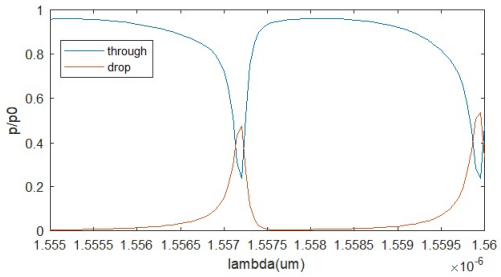

Figure 2.2: The spectrum of the simulated 2D ring resonator

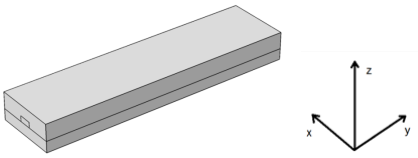

Figure 2.3: Geometry of the simulated waveguide: Core width= 500nm, core heigth= 220nm, cladding width= 2.5um and cladding height= 1.1um

and the model will solve according to Eq.2.3 for βy , βx and βz.

$$E = E_0 e^{-j\beta y} \tag{2.3}$$

Here we are only interested in a field which has been excited orthogonal to the zx surface, therefore we model by βy.

If we excite the port with TE or TM mode we will have different results. if we sweep the refractive index of the solution which is on top of the core, we will retrieve the corresponding effective refractive index at each point. Considering the fact that more n_{eff} changes will result in higher wavelength shift; we can say, it will be satisfying if we excite a particular mode that has more evanescent filed on top of the core where the solution is present. TE mode will have evanescent field more centered at the right and left sides of the core; however, TM has evanescent field centered at the top and bottom of the core. See fig 2.6.

We will check the sensitivity of our micro ring resonator with TE and TM mode excitation. By sweeping the refractive index of the solution from 1.33 to 1.4 we can obtain β_y corresponding to the relative refractive index. We are actually using β_y to retrieve n_{eff}. Considering the input light to be at wavelength equal to 1.55um and by knowing β we can easily derive n_{eff} by using eq.2.4.

$$\beta = n_{eff}(2\pi/\lambda) \tag{2.4}$$

With every corresponding n_{eff} that we obtain by sweeping the refractive index of the solution we can plot a graph as can be seen in fig 2.7

According to eq.1.1 for each of these refractive indexes we can calculate the resonance wavelength. Afterwards by using eq.2.2 we can calculate the sensitivity. In eq.1.1 the multiplier "m" indicates in which period you are looking for the

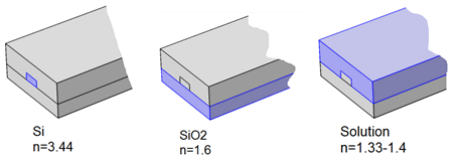

Figure 2.4: The materials and their corresponding refractive indexes

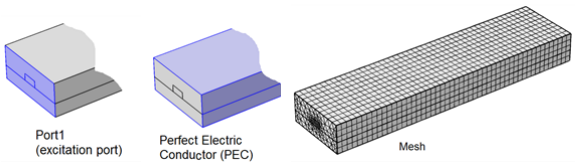

Figure 2.5: Excited port, the PEC defined and the mesh used

wavelength resonance. This means before any calculation we need to find the integer value m corresponding to the period that we are looking for our resonance wavelength.

we know that:

$$\beta L = 2\pi m \tag{2.5}$$

where L is the length of the path in which light is propagating and m is the period that we are operating in. Since we are simulating with $\lambda = 1.55um$ and the propagation path is assumed to be a ring (for ring resonator) with radius r=40um, therefore the period can be calculated as :

By substituting eq.2.4 in eq.2.5 and by considering that L=$2\pi r$, r=40um and λ= 1.55um, we conclude that "m" is equal to 389. Now if we substitute the value 389 instead of "m" in eq.1.1 we can calculate the resonance wavelength. By looking at fig 2.7 we see that n_{eff1}= 2.4015 and n_{eff2} = 2.4125. We can calculate the lambda shift by inserting n_{eff1} and n_{eff2} in eq.2.5, therefore $\lambda 1 = 2\pi n_{eff1} r/m$ and $\lambda 2 = 2\pi n_{eff2} r/m$ Then, $\Delta\lambda = 7.07nm$ Keep in mind that we have swept the refractive index of the solution from 1.33 to 1.4, therefore $\Delta n_{solution} = 0.07$. By eq.2.2 we can calculate the sensitivity of a micro ring resonator that has been excited in TE mode. $S_{TE} = 101nm/RIU$

We have already checked the sensitivity by sweeping the refractive index of the solution. Since we are interested into improving optomagetic technique, we must model our system with DNA and a bead on top of it. So we decided to simulate a channel waveguide with both TE and TM excitation modes. The difference is that this time we model the bead and we slightly move down the bead from very far away from the surface of the ring to the closest point to the surface, instead of sweeping the refractive index of the solution. In this way we exactly see how much n_{eff} changes if by any means we move down the bead close enough to the surface. The bead is modeled with 2 circles with radius of 39nm and 65nm. The inner circle represent the monoxide core which has real refractive index equal to 2.4460 and the outer circle is made of dextran with 1.34 refractive index [4].

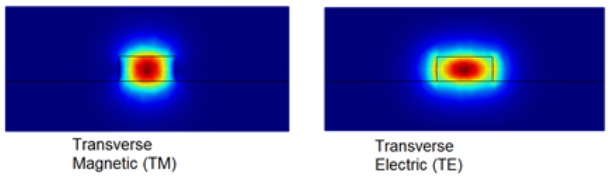

Figure 2.6: In TE mode the evanescent field is less confined at the top and bottom of the core; however, in TM it is the opposite.

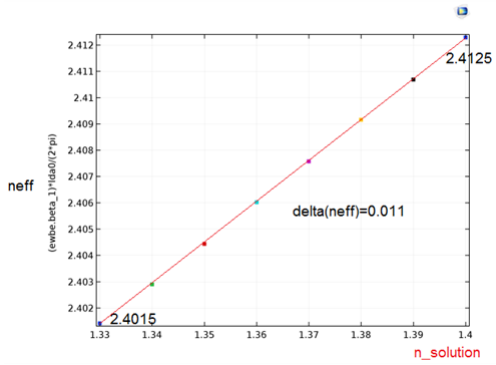

Figure 2.7: n_{eff} corresponding for $n_{solution}$= 1.33 is 2.4015 and for $n_{solution}$= 1.44 is 2.4125 in TE mode

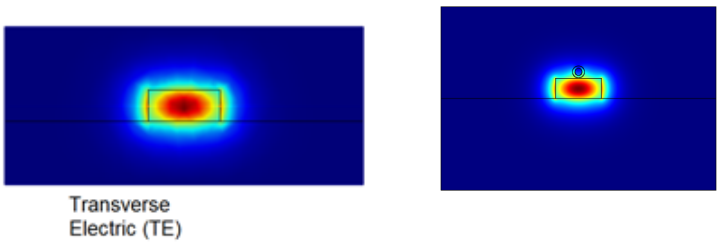

Figure 2.8: The image on the left in TE mode without the presence of bead and on the left side we have illustrated the full model considering the effect of the bead at its closest point to the ring

If we define the distance of the bead to the surface of the ring as "d" and sweep the parameter d from 200nm to 5 nm we will find out huge sensitivity difference between TE and TM mode. See fig 2.9.

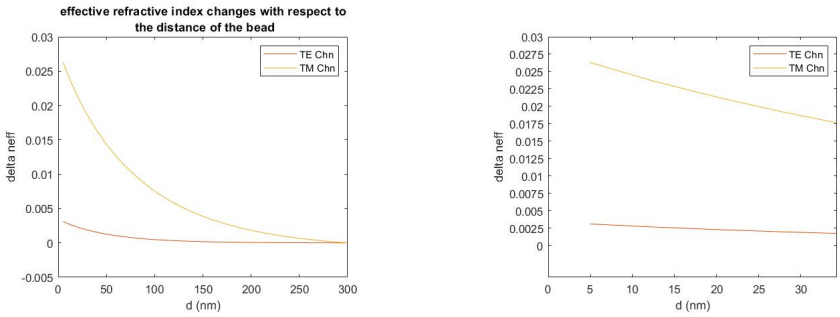

Figure 2.9: Δn_{eff} with respect to the distance of the bead (d)

In real case scenario the distance of the bead starts from 20nm since the length of the bead is almost 20nm. Δn_{eff} in TE mode is around 0.0008 from 20 nm to 5 nm; however, in TM mode Δn_{eff} is around 0.005 which means at least 6 times better than using TE mode excitation. Taking As an example the wavelength shift that we could obtain previously by using a passive bead and TE mode excitation as can been seen in 1.5 was around 500pm; however, in our case the sensitivity improvement by exciting TM mode will promote this wavelength shift upto 3nm. This will help us detect even less concentration that we didn't use to detect easily. Consider that the values of the Δn_{eff} mentioned above must be normalized since the simulation has done in 2D and what we desire is the refractive index changes of a single bead. The refractive index changes of a single bead is $3.18e^{-7}$ for TE excitation and $2e^{-6}$ for TM excitation.

This is interesting that we can promote our system by bringing down the bead and using TM mode excitation. However, the question is how we can bend DNA in order to minimize the distance of the bead with the surface of the ring. To answer this question we need to study about the characteristics of DNAs and their mechanical properties in order to find out what amount of force we need to provide to completely bend DNA, which we will discuss in the next section.

2.2 DNA Bend Model

DNAs dependant on their length have different mechanical characteristics. Here as we want to figure out the amount of force that is required to bend the DNA, we are only interested in the mechanical properties of DNA. Considering the length of DNA, we can classify them into DNAs that are longer than their persistence length and the ones that are less than persistence length. If we apply a force to a DNA that is longer than its persistence length, the only thing we can say about the shape of the DNA after a while is the end to end distance of the DNA which is calculated by monte carlo, random walk model which is completely statistically. For instance if we apply a force to one end of DNA with a specific angle at last we can say with probability of "p" the end to end distance of the DNA is bigger than a specific number [5].

In another case if the length of the DNA is less than its persistence length, then we can model it as a bar or spring or polymer. Therefore we can calculate the deterministic end to end distance of a DNA. The reason is the Thermal energy

K_BT. The thermal energy will bend, stretch and squeeze DNAs that are longer than their persistence length. However, in shorter DNAs the rigidity will prevent K_BT to freely affect the end to end distance of the DNA.

$$\zeta_p = \kappa / K_BT \tag{2.6}$$

Where ζ_p is the persistence length of DNA and κ is the rigidity of the filament.

According to the rigidity of the DNA and the thermal enery to be 4pN nm which is 0.6kcal/mol, the persistence length of a DNA will be around 50nm. Each base pair of DNA is around 0.3 nm therefore the persistence length of DNA is said to be around 150 base pairs. In our case the length of the DNA is 20nm (60bp) which means it is less than persistence length.

For DNAs that are short in vertical direction, if we apply a force horizontally in presence of thermal energy then DNA bends over a curvature of radius R according to eq.2.7.

$$F_{bend} = 1/2 K_BT \zeta_p R^{-2} \tag{2.7}$$

F_{bend} is the force that is applied to one end of DNA that has rigid connection in the other end. As an example if we apply 0.12pN force to one end of DNA with any lenght, it bends over a curvature of radius 29nm.

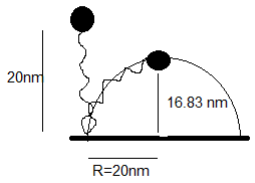

Figure 2.10: If we apply $2.56e^{-13}$ force to the bead, DNA will bend over a curvature with radius R= 20nm, therefore the distance of the bead with the surface of the ring will decrease from 20nm to 16.83

If we plot eq.2.7 for a DNA with length 20 nm, we can plot the position of one end of DNA with respect to the force applied to this point.

Figure 2.11: Distance of the bead located on top a DNA with length 20nm from the surface of the ring resonator

Now we want to see if we can model DNA in a way that by applying a range of different forces to one end of DNA it bends down similar to fig 2.11. In this case we

validate our model and we can use it in order to apply any arbitrary force and see how it affects the DNA mechanically.

DNAs are made of base pairs that each one can be modeled as hinge joints with rotational spring and damping effect. The simulation has been done by Comsol Multi physics studying at stationary state using Solid Mechanics as the physics behind it. By sweeping the parameters k and c for some particular forces we can check with fig 2.11 to validate the model by finding parameters k and c to match simulation with theory. After simulation the best fit to this model is k= $1e^{-19} N.m/rad$ c=$1e^{-16} N.m/rad$ where k is the rotational spring constant and c is the damping coefficient.

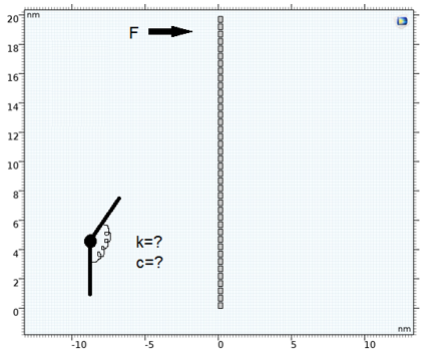

Figure 2.12: DNA is modeled by 60 hinge joints where the force is applied horizontally to the top end of DNA where beads are supposed to be connected here. The other end is fixed as a rigid connector, the question is what should be the values of spring constant (k) and damping coefficient (c)

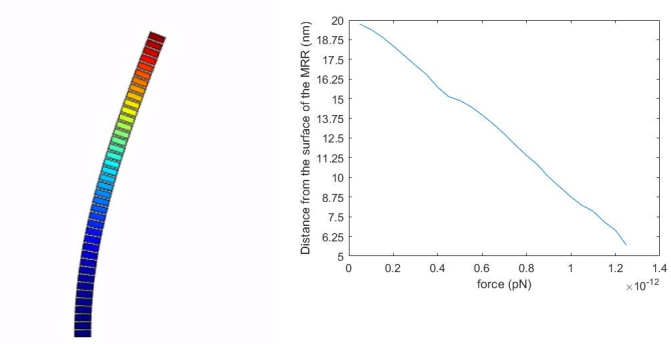

Figure 2.13: The result of simulating a DNA with hinge joints as its basepairs with k=$1e^{-19} N.m/rad$ and c=$1e^{-16} N.m/rad$

By comparing the two figures they match pretty good with each other, therefore our model is almost verified. Now we know what force with whatever angle it has will bend DNA, and therefore we can now simulate the position of the bead after applying an arbitrary magnetic force. This is helpful in the following chapter where we will seek for an optimized magnetic coil structure. Because we are willing to see how this magnetic force can bend DNA, we can find an optimized structure that produces force in such condition that completely bends DNA effectively. In this case we can maximize the effective refractive index shift and in conclusion we maximize the resonance wavelength shift.

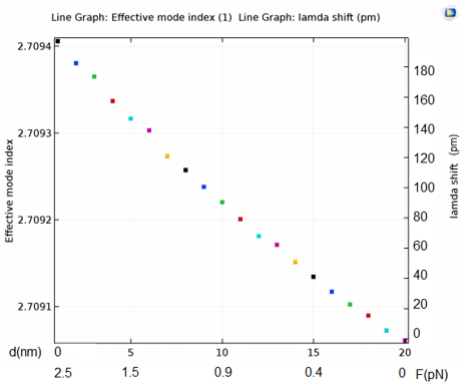

Figure 2.14: n_eff shift and wavelength shift with respect to the horizontal magnetic force applied to bead on DNA with 20nm lenght

Fig 2.13 shows our progress clearly. in this figure we conclude that if we manage to apply a force of around 1pN, we will bend DNA in such a way that bead touches the surface of the ring and it yields a resonance wavelength shift of 100pm. Keep in mind that this simulation has been done by exciting the waveguide with TE mode. Consider exciting TM mode the resonance wavelength shift would be 600pm more than what we could get from passive labelling approach.

In the next chapter we will look for an optimization path to find out the best structure that can provide an almost horizontal magnetic force of 1pN on the magnetic bead.

Chapter 3

Magnetic Coil Design

3.1 Towards Magnetic Integration

We saw in the previous chapter that how an applied force can bend DNA over a curvature towards the surface of the micro ring resonator or in another point of view we saw as a result the amount of force need to be applied in order to completely bend the DNA is something around 1pN. This rises the question to check the possibility of finding a structure of a magnetic coil to be not only able to provide this amount of force, but also integrated inside a photonic chip where the ring resonator is also present, this means the magnetic coils must be almost the same size as the ring resonator or at least the same order of magnitude.

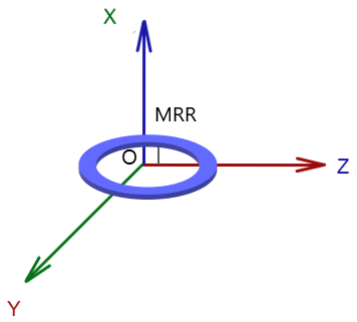

Figure 3.1: Ring resonator is the blue ring illustrated in x,y,z Cartesian coordination

If we establish a coordination of x,y,z where ring resonator is fixed at x=0 and then look at the system from y in xz plane. we can see the ring resonator as in fig 3.2.

The system is symmetric with respect to z axis therefore let's focus on the right side. We saw in previous chapter that how a horizontal force applied to the bead can bead DNA, so let's discuss on how it is possible to have such magnetic force with such angle. if there exists a particle with ferromagnetic characteristics inside a non uniform magnetic field it moves toward the points where the density of the field is higher, therefore we can easily say in order to have a horizontal magnetic force on the ferromagnetic bead which is bound to the end of DNA requires a field that its density is increasing as we get further on z direction.

As can be seen in fig 3.3 a magnetic field as illustrated can provide a horizontal magnetic force on the bead. If we go back to x,y,z coordination where we saw the

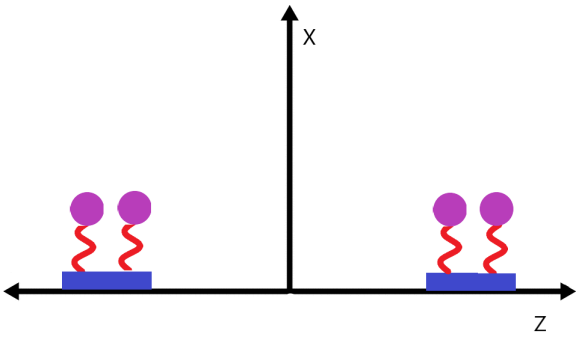

Figure 3.2: Schematic illustration of ring resonator in 2D

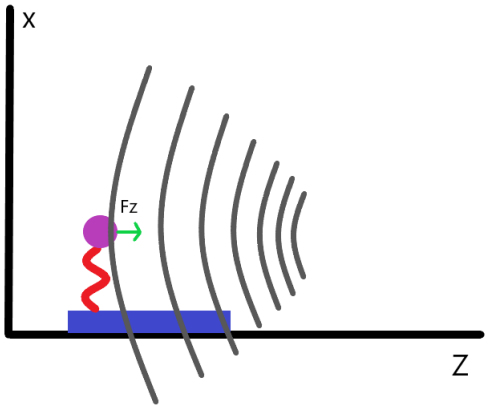

Figure 3.3: Magnetic field illustrated in black can generate F_z which is of our interest

complete ring resonator in fig 3.1 and we install a solid metal ring with current flowing inside, and with inner radius larger than ring resonator we can generate a magnetic field we desire that can be seen in fig 3.4.

Taking this 2D structure that can bee seen in xz plane in fig 3.4 as the basic one and try to build as many different combinations of ring and coil based on the basic structure will lead us to the optimized final configuration. The possible structures that can be built based on the basic one are as following.

Since The structures are symmetric with respect to x axis therefore the simulation can be done using 2D axisymmetrical simulation. What we can change in these different structures are only 2 things. 1-the current density flow inside the coils. It is very clear that having more current density flow will generate higher magnetic field. 2- The inner radius of the coils or better to say the distance between the coil and the ring resonator. this is also very clear that the closer the coil to the ring the more magnetic field amplitude on the bead.

By sweeping these two parameters and run the simulation on all the possible structures will result in two values; the amplitude and the angle of the force. However, this simulation doesn't give the force on the bead since the characteristics of the ferromagnetic bead and its dimension is individual, therefore the further calculations are done by hand. What we obtain by this simulation is the magnetic field (H) generated by the magnetic coils.

$$F_{magn} = 1/2\mu X V_{bead} \nabla H^2(r0) \tag{3.1}$$

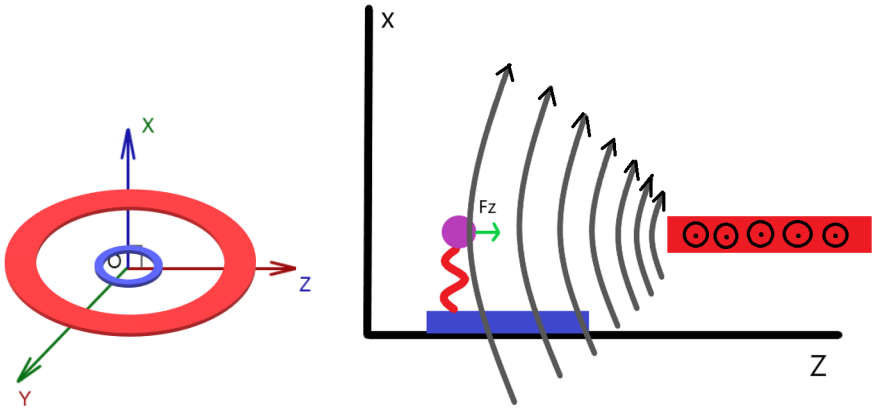

Figure 3.4: MRR is illustrated in blue, while the magnetic coil is illustrated in red

where μ is the permeability of the magnetic bead, X is the susceptibility of the magnetic particle and the gradient of squared magnetic field must be calculated at r0 where the bead is located. V_{bead} is also the volume of the bead. All these values except the ∇H^2 are constants that are dependant on the characteristics of the bead. What we need to study is the $\nabla H^2(r0)$ that we can obtain on the bead in different test structures.

$$\nabla H^2 = \nabla(H^T H) \tag{3.2}$$

$$H = H_x \hat{a_x} + H_y \hat{a_y} + H_z \hat{a_z} \tag{3.3}$$

$$H^T H = \begin{pmatrix} H_x \\ H_y \\ H_z \end{pmatrix} \begin{pmatrix} H_x & H_y & H_z \end{pmatrix} = \begin{pmatrix} H_x^2 & H_x H_y & H_x H_z \\ H_y H_x & H_y^2 & H_y H_z \\ H_z H_x & H_z H_y & H_z^2 \end{pmatrix}$$

$$\nabla H^T H = \partial/\partial x H^T H \hat{a_x} + \partial/\partial y H^T H \hat{a_y} + \partial/\partial z H^T H \hat{a_z}$$

Assuming that $H_y = 0$ which is orthogonal to the plain of our study which is xz then we can say:

$$\nabla H^T H = \begin{pmatrix} \partial/\partial x & \partial/\partial z \end{pmatrix} \begin{pmatrix} H_x^2 & H_x H_z \\ H_z H_x & H_z^2 \end{pmatrix}$$

Therefore we can finally calculate ∇H^2 at any point in the xz plane.

$$\nabla H^2 = \hat{a_x}(\partial/\partial x H_x^2 + \partial/\partial z H_z H_x) + \hat{a_z}(\partial/\partial x H_x H_z + \partial/\partial z H_z^2) \tag{3.4}$$

With this vector decomposition we have all the elements required for simulating the magnetic coils and the following magnetic forces.

3.2 Simulation of the Magnetic Coil

The derived vector will be used to calculate both the amplitude and the angle of the force by putting the magnitude and the angle of the vector in eq.3.4 and substitute it in eq.3.1. We simulate the 5 different structures illustrated in fig 3.5 by using Comsol Mutiphysics. The simulation is done in 2D axisymmetrical geometry, the physics used is "magnetic fields", and we study in stationary mode. The current

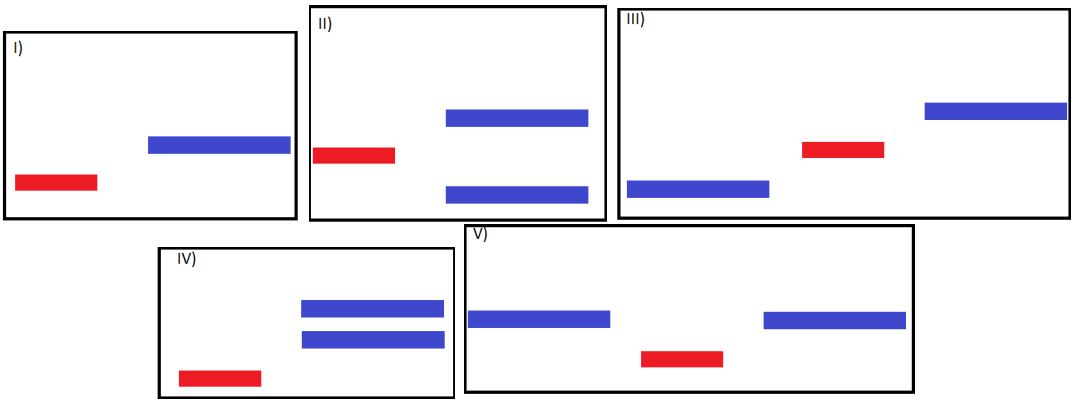

Figure 3.5: 5 different structures composed by the basic structure. All blue coils have 10[um] width and 750[nm] height. All the red ring resonators have 220[nm] height and 500[nm] width.

that flows inside the coil in 100mA and it is flowing inside the plane as in fig 3.4. The width of the coil is 10um and the height is 750nm. Let us call the inner radius of the coil as parameter "r" and at the initial state as seen in fig 3.5, "r" is 45.5um.

The inner radius of the ring resonator is 40um and its width is 500nm, while its height is 220nm. Simulating the first structure in fig 3.5 and considering the eq.3.4 we can derive the angle of the force which is equal to the angle of ∇H^2 and the magnitude of the force which is proportional to the magnitude of ∇H^2 with same proportion for all the different structures.

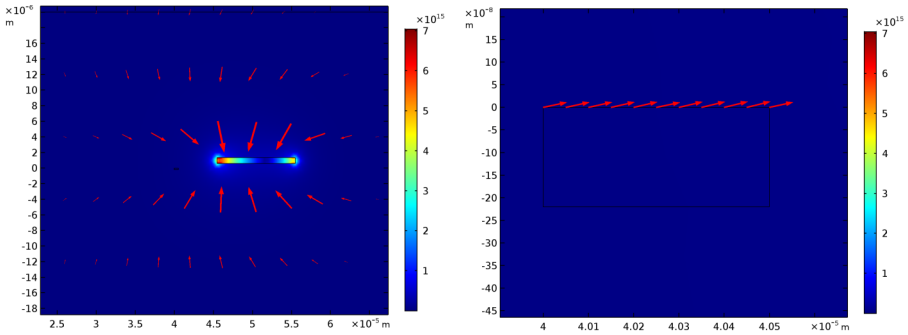

Figure 3.6: The angle of the gradient generated by the first structure can be seen in both images, while the right image is zoomed on the surface of the ring resonator

The angle of the force that can be generated by the structure-1 can be seen in fig 3.6. which is almost horizontal.

The magnitude of the gradient obtained by structure-1 on the surface of the ring resonator is around $5e^{13}$. The classic structures we used to use for active labelling as can be seen in fig 1.7 could generate $1e^{10}$ which is 3 orders of magnitude lower than what we can obtain by this structure today. We can see in fig 3.7 that this gradient is not the maximum that we can obtain and it looks like we can generate even more force if we drag the magnetic coil closer to the ring resonator. Also it is obvious that the current applied to the coil which is 100mA is playing a role in defining the magnitude and the angle of the gradient. We run the simulation once more by sweeping the inner radius of the coil for values of "40.5, 41.5,42.5,43.5,44.5 and 45.5". This means we are actually sweeping the distance of the coil from the

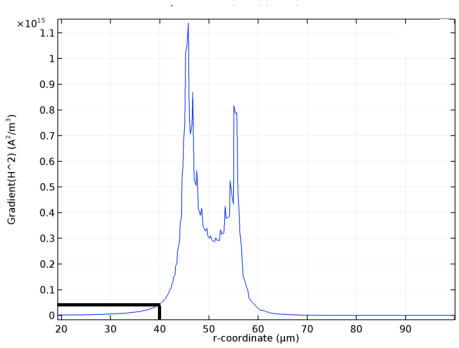

Figure 3.7: The magnitude of the gradient generated by the first structure. At point r=40.11um which is on the surface of the ring resonator the gradient is $5e^{13}$

ring from 5 [um] to 0 [um] which is the closest point to the ring resonator. Let us consider the current density flow in the first structure with 100mA to be "J". We sweep each structure for each inner radius, different current density flows as "J, 1.4J, 2J and 4J". Simulating on all the 5 different structures will lead us to choose the best structure according to the maximum force amplitude, with angle closest to the horizon.

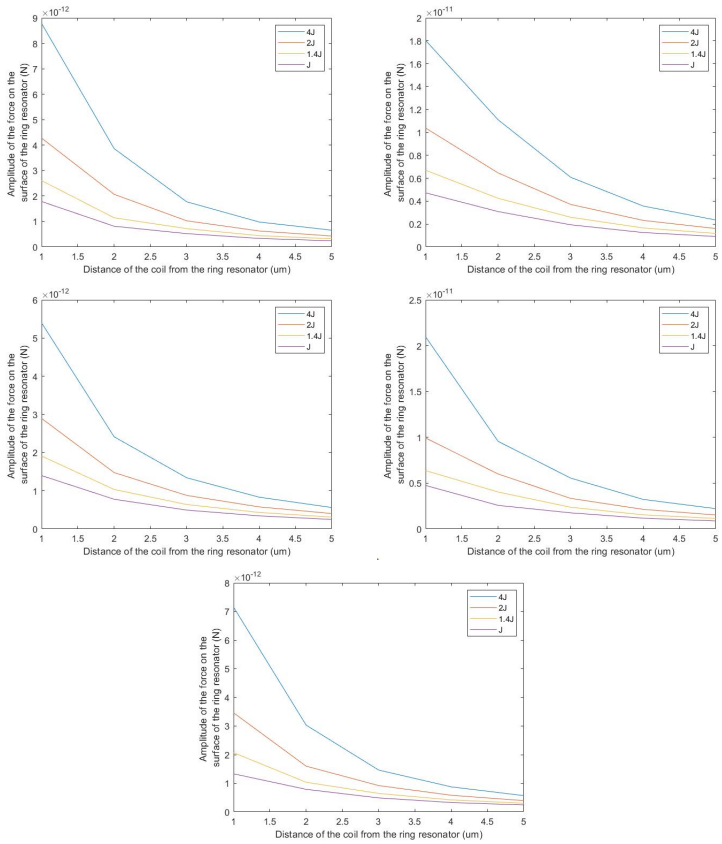

Figure 3.8: Amplitude of the force for 5 different structures on the surface of MRR for different current density flows

If we consider the amplitude and the angle of the force , we can conclude that the first structure can generate the most effective force on the bead (see fig 3.8 and fig 3.9) close to the surface of the ring. Which is satisfying since the first structure

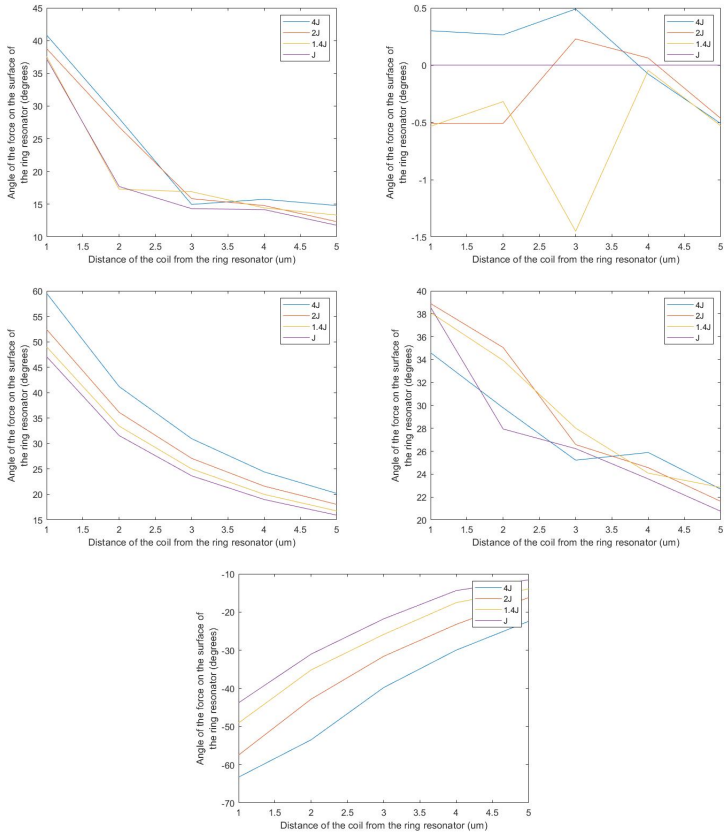

Figure 3.9: Angle of the force for 5 different structures on the surface of MRR for different current density flows

is easier to implement than the other 4 according to the layers we need to dig, in the wafer of the chip. The force we obtain can completely bend DNA in order to bring the bead at the closest point to the surface, this amount of force is 3 orders of magnitude larger than the classic active labelling procedure. Although the force we obtain at the furthest distance of the coil, and the least current density flow can not fully bend DNA to the surface; however, the bead can touch the surface due to its large dimension. The most progression we are interested in apart from improvement of the wavelength shift is the integration of the coil and the ring resonator at one chip. You can see in fig 3.8 that we can even arrive very close to 60pN if we inject 4J current density flow. Therefore it is also very important to check the capability of the magnetic coil with dimensions mentioned above to handle such current density flow. Or in other words in the next chapter we will check the maximum current density flow we can reach in the first structure and we will discuss on how we have designed the board for implementing the whole system.

Chapter 4

Experimental Setup

We had the possibility to access a multi project wafer run in order to fabricate a sample chip and perform early stage tests on the concepts described in the the previous chapters. In the previous chapter we saw how we increased the force applied to the ferromagnetic bead by integrating the magnetic coil inside the photonic chip. We wish we could also integrate the electronic board which drives the coils inside the photonic board; however, it is not possible at the moment. Since the photonic chip is in contact with the solution we want to do the experiment on, and it prevents us to have all the photonic and electronic board integrated at least into one board, if we don't say into one integrated chip right now. In the other words we say we have one photonic board and one electronic board separated from each other and connected by a third board, called connector.

4.1 Coil Characterization Inside the Photonic Chip

We have to check the coil characteristics like resistance and max current it can hold. In order to check the capability of the coils we use a voltage supply that can provide current upto 500mA. By putting in series a variable resistor and reading the current which is equal to the current flowing inside the coil, we can obtain the resistance of the coils. The voltage we apply is a DC voltage, therefore we can check only the resistance of the coil. To check the inductance and capacitance of the coil we can use a sinusoidal function generator. The experiments reveals that current remains steady as we change the input frequency of the sinusoid, therefore the coils only have same characteristics of a resistor with no inductance and capacitance.

Experimenting on the resistance of the coils with DC input voltage reveals that the coils are at most 10 and at least 6 Ω. (see fig 4.1)

By inject more current into the coils we can see after injecting 300mA the coil in structure-2 has been burnt. See fig 4.2 and fig 4.3.

We are going to experiment structure-1 inside the photonic chip which is similar to the basic structure in chapter 3. 300mA that we can inject inside the coil means we can reach to 3J density flow in fig 3.8 in structure 1 which means we can reach to 1pN at the worst case and we can reach to 10pN at the best case.

The ring resonator inside the chip for the first 3 structures has inner radius equal to 40[um]; however, the last structure has 80[um] inner radius. The technology is silicon and the core of the MRR is Si while the substrate is SiO_2. The width of the ring is 220[nm] and the width is 500[nm]. The excitation mode inside the core

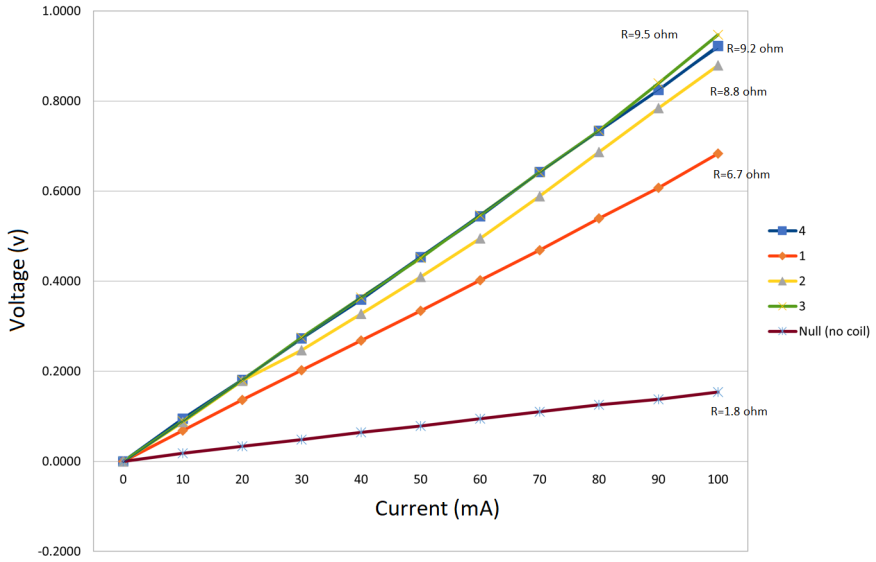

Figure 4.1: The v-I (Voltage-Ampere) curve of the 4 structures and at the null state where no coil is present in the photonic chip

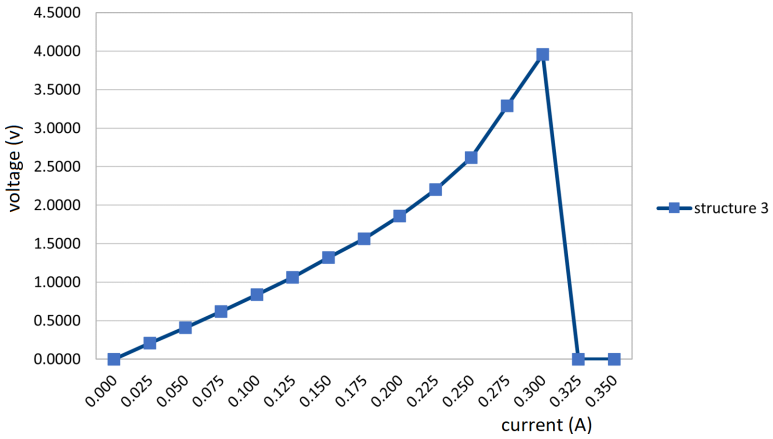

Figure 4.2: The maximum current that we are able to apply to the coils is atmost 300mA

is TM. As we discussed before TM is more efficient for sensing the refractive index variations on top cladding since the evanescent filed in more confined at the upper and lower side of the core.

The first structure (see fig. 4.3) is the same as the basic structure designed in the previous chapter.

The dimensions of structure 2 is as following:

structure-2:

R=40[um] (inner radius of ring resonator)

width-R= 500 [nm] (width of the ring resonator)

height-R=220[nm] (height of the ring resonator)

this structure has got two coils with:

coil1:

R=47.5[um] (inner radius of coil)

width-c=8[um] (coil width)

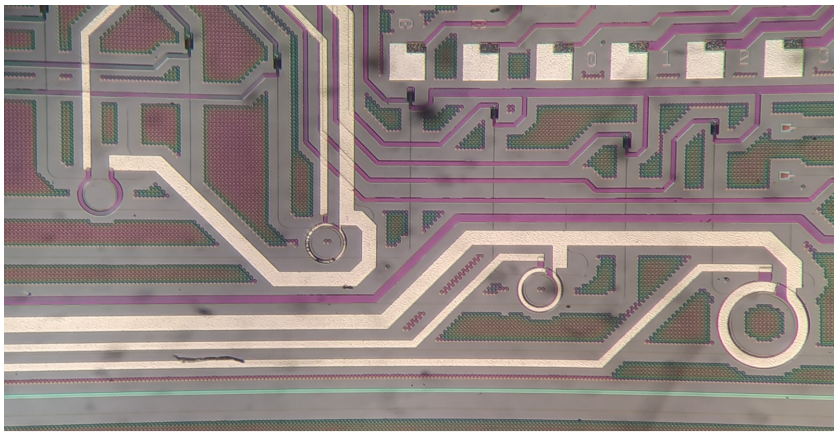

Figure 4.3: Coils and MRR inside the chips are labeled from left to right from 1 to 4. The second structure has been burnt due to maximum current injection

height-C=750[nm] (coil height)
coil2:
R=49[um] (inner radius of the coil)
width-c=5[um] (coil width)
height-C=2[um] (coil height)
coupling gap = 300[nm]

structure-2, 3 and 4 are similar to design number 4 in fig 3.5 where we had 2 coils on top of each other above the ring resonator. In that case we could obtain high force amplitude (see fig 3.8). The idea behind using the same structure with 3 different dimensions is that we can inject different current flows due to their difference in dimensions.

Structure-3:
R=40[um] (inner radius of ring resonator)
width-R= 500 [nm] (width of the ring resonator)
height-R=220[nm] (height of the ring resonator)
this structure has got two coils with:
coil1:
R=47.5[um] (inner radius of coil)
width-c=10[um] (coil width)
height-C=750[nm] (coil height)
coil2:
R=49[um] (inner radius of the coil)
width-c=15[um] (coil width)
height-C=2[um] (coil height)
coupling gap=350[nm]
Structure-4:
R=80[um] (inner radius of ring resonator)
width-R= 500 [nm] (width of the ring resonator)
height-R=220[nm] (height of the ring resonator)
this structure has got two coils with:
coil1:
R=87.5[um] (inner radius of coil)
width-c=25[um] (coil width)

height-C=750[nm] (coil height)
coil2:
R=89[um] (inner radius of the coil)
width-c=30[um] (coil width)
height-C=2[um] (coil height)

4.2 Photonic Board

This board contains two main components. 1-the photonic chip is a 16 pin-one-sided chip that is connected to 4 coils and 4 ring resonators inside itself. Each ring resonator has 2 out comes as through port and drop port. The photonic board is designed in order to hold the photonic chip and the fluidic cell. As can be seen in fig. 4.4 the holes are designed according to the fluidic cell and it can be fixed on top of the photonic chip.

Figure 4.4: This board is designed by Altium designer 20.0.2

As can be seen in fig 4.4 16 pins of photonic chip that contains 4 structure of coils and 4 ring resonators are routed to PCI 36 pin flat connector. The connector board is used to connect the photonic board output as PCI 36 pins to the electronic board as flat cable. It contains 2 components overally with its routing in between.

4.3 Electronic board

This board contains 8 main components not considering the corresponding capacitors, resistors and connectors. It is designed for driving the coils, driving the photodiodes, reading the photodiodes and reading the current flowing inside coils.

The 4 Trans Impedance Amplifiers (TIAs) are for reading 8 photodiodes that are connected to the data acquisition with a pin connector. Each ring has one through port and one drop port. Therefore 4 rings will require 8 photodiodes.

The 2 Inas are used for 4 magnetic coils in order to read the current flowing inside the coils, we have to keep in mind that this value must not exceed 300mA otherwise the coil will burn. The current is acquired by a shunt resistor parallel to

the Inas which is 1 Ω in order to not consume a lot of energy. And it can not be less since in the data sheet of using these ICs is written that this resistor can not be very low.

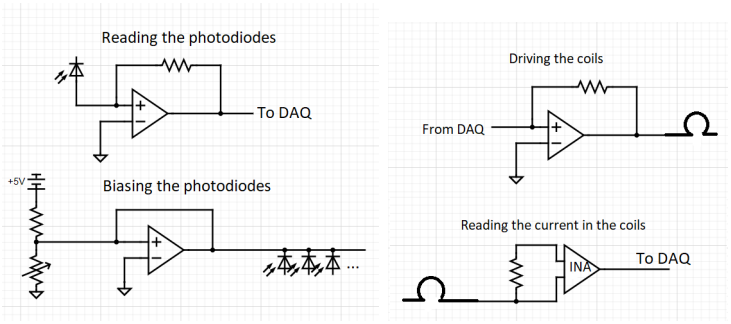

Figure 4.5: Schematic drawings of the 4 different circuits that are in the electronic board: 1- reading the photodiodes 2-biasing the photodiodes 3-driving the coils 4-reading the current flow in the coils

We need 4 op-Amp in order to drive the coils and we use AD8534 IC that has 4 op-Amps integrated inside.

Another buffer is needed in order to drive the cathode of the photodiodes. All photodiodes are activated by one circuit.

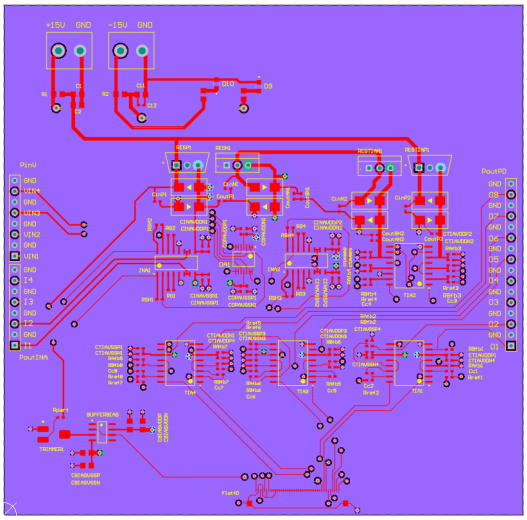

Figure 4.6: The electronic board that is designed by Altium Designer 20.0.2. This board reads the photodiodes and activates the cathode, while it drives the coils and reads the current flowing inside the coils. the

Conclusion

In the field of bio sensing that uses photonic micro ring resonator as a mean for sensing, we designed an integrated system of MRR with magnetic coil, that has a significant improvement in comparison with the older version where we used to use magnetic coils outside the photonic chip.

Integration in this case will result in higher sensitivity of the sensors which is a very important figure of merit as far as we are working with sensors. Sensitivity in our case measures how much the resonance wavelength shifts if we have a certain variation of refractive index. By integrating the photonic ring resonator with the magnetic coil, we can increase the force applied on the bead by 3 orders of magnitude which will result in 6 times more resonance wavelength shift for the same concentration of analytes.

In this system our bio sensor is more effective and efficient. The point is that when we had a magnetic coil outside the system, we could not certify if the location of the ring with respect to the location of the magnetic coil stays stable. This happens a lot when we are doing measurement in the lab even under very strict circumstances. We have designed the electronic board and photonic board and everything is ready for doing measurement to see how far we can get low in the concentration.

The improvements that can be done is in the integration of the electronic board and the photonic board. The reason that prevents us from designing such board is that the photonic chip must be in contact with the solution where we have the analytes. This can be solved by setting up the photonic chip far away from the electronic components on the chip. However, this will result in designing a very big board with several connectors that will decrease our order of freedom. Pushing the envelope in this criteria will be Integrating the photnic board and the electronic board in one single chip.

Bibliography

[1] A. Jebelli, F. Oroojalian, F. Fathi, A. Mokhtarzadeh, and M. d. l. Guardia, "Recent advances in surface plasmon resonance biosensors for microRNAs detection," *Biosensors and Bioelectronics*, vol. 169, p. 112599, 12 2020.

[2] E. Yablonovitch, "Photonic crystals," *Journal of Modern Optics*, vol. 41, no. 2, pp. 173–194, 1994.

[3] Q. Xu and M. Lipson, "All-optical logic based on silicon micro-ring resonators," *Optics express*, vol. 15, no. 3, pp. 924–929, 2007.

[4] M. Holzinger, A. Le Goff, and S. Cosnier, "Nanomaterials for biosensing applications: a review," *Frontiers in chemistry*, vol. 2, p. 63, 2014.

[5] H. G. Garcia, P. Grayson, L. Han, M. Inamdar, J. Kondev, P. C. Nelson, R. Phillips, J. Widom, and P. A. Wiggins, "Biological consequences of tightly bent dna: the other life of a macromolecular celebrity," *Biopolymers: Original Research on Biomolecules*, vol. 85, no. 2, pp. 115–130, 2007.